International Journal of Current Engineering and Technology
E-ISSN 2277 – 4106, P-ISSN 2347 – 5161

Available at http://inpressco.com/category/ijcet

Research Article

Design of O-Ring with No-Groove Arrangement

S M Muzakkir

Department of Mechanical Engineering, Jamia Millia Islamia, New Delhi, India

Received 10 May 2022, Accepted 10 June 2022, Available online 16 June 2022, **Vol.12, No.3 (May/June 2022)**

Abstract

The O-rings are the very commonly employed solution for creating sealing to prevent the loss of pressurized fluid or gases. In the present work the design of an O-ring with no-groove arrangement is presented.

Keywords: *Lubricated O-ring, Un-lubricated O-ring, Sealing, Design, Leakage, Elastomers*

1. Introduction

The loss of pressurized fluid or gas is generally prevented by the use of O-rings. The O-rings are made up of elastomeric materials. The sealing effect in these elastomers occurs due to their axial or radial compression. The elastomer behaves as an incompressible liquid of great viscosity with high surface tension [1]. When the O-ring is installed in such a way that no groove has been provided in the assembly, then this type of arrangement is called no groove arrangement [2]. There are two types of no groove arrangement, depending upon the type of compression being imposed upon the O-ring, the Axial O-ring and Radial O-ring [3].

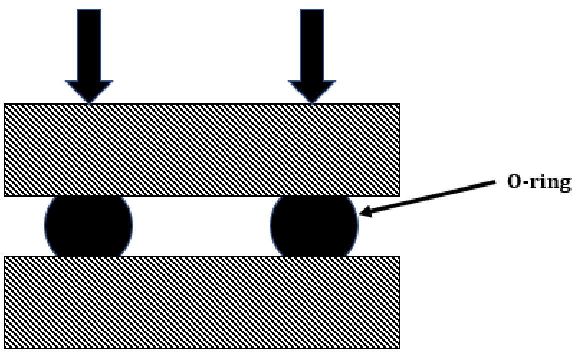

Fig.1 Axially loaded O-ring without groove

The no groove arrangement for the axial loaded O-ring is depicted in figure 1. Under the case of axial compression, the O-ring is free to expand radially as a result of which the corresponding shape of the O-ring under load changes as shown in the figure 2.

*Corresponding author's ORCID ID: 0000-0003-4280-9361
DOI: https://doi.org/10.14741/ijcet/v.12.3.6

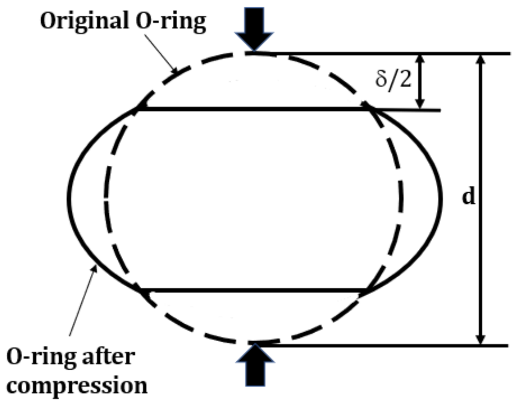

Fig. 2 Deformed O-ring

The compression brings out a change in the cross-sectional diameter of the O-ring, from an initial value of 'd'[2]. In order to define the change in the diameter, a parameter called as compression ratio (ψ) is introduced which is defined as the change in the cross-sectional diameter divided by the original cross-sectional diameter.

$$\psi = \frac{Change\ in\ cross-sectional\ diameter}{Original\ diameter} \quad (1)$$

The analysis of the O-ring has been divided into two categories, namely: (i) Unlubricated condition and (ii) Lubricated condition based upon whether lubrication was provided to the O-ring prior to its installation within the assembly or not [4], [5], [14]–[23], [6], [24]–[33], [7], [34]–[43], [8], [44]–[53], [9], [54]–[63], [10], [64]–[69], [11]–[13]. Lubrication may result in swelling up of the O-ring, which increases the cross-section diameter of the O-ring.

2. Axially Loaded Unlubricated Condition

The unlubricated condition specifies the situation when the O-ring has been installed in the assembly without prior lubrication around the surface of the O-ring. In static applications, where movement between the sealing faces and the O-ring is negligible, unlubricated O-rings can be utilized without significantly affecting the life of the O-ring.

Squeeze upon loading: The O-ring under compression will undergo an effective squeeze defined as the change in its cross-section which is calculated from the compression ratio (ψ) and O-ring diameter (d).

The formulation is given in equation 2.

$$squeeze = \psi * d \quad (2)$$

There are two approaches for the calculation of Young's Modulus.: Young's Modulus determination using hardness and the other using stress and strain values

Young's Modulus determination using hardness: The estimation for Young's Modulus has been formulated using the value of hardness as a parameter using the empirical relation proposed:

$$E = 0.256 * e^{0.047*(hardness-hardtol)} \quad (3)$$
$$E = 0.256 * e^{0.047*(hardness+hardtol)} \quad (4)$$

When calculating Young's Modulus using hardness, both positive and negative tolerances have been utilized in the O-ring design leading to two different values of Young's Modulus. Under the same compression imposed upon the O-ring, positive tolerances on hardness yield a higher value of Young's Modulus and consequently the stresses generated on the O-ring will be higher and vice versa. Therefore, for calculating the stress, positive tolerance of O-Ring is considered and in the case of safeguard against leakage/squeezing out, calculation of Young's Modulus using negative tolerances is incorporated.

Young's Modulus determination using stress and strain values: The estimation of Young's Modulus using hardness as a parameter is based on an empirical relation and therefore, in order to estimate a more accurate value of Young's Modulus, stress and strain values, which have been arrived experimentally are preferred.

The relation between stress and strain for hyper-elastic rubber materials such as O-ring is non-linear, and several models have been proposed from time to time in order to evaluate the value of Young's Modulus using stress and strain.

According to Cauchy-Green, the stretch imparted to any material can be expressed by using three invariants as represented below:

$$I_1 = \lambda_1^2 + \lambda_2^2 + \lambda_3^2 \quad (5)$$
$$I_2 = \lambda_1^2\lambda_2^2 + \lambda_2^2\lambda_3^2 + \lambda_1^2\lambda_3^2 \quad (6)$$
$$I_3 = \lambda_1^2\lambda_2^2\lambda_3^2 \quad (7)$$

Where λ represents the stretch and is defined as:

$$\lambda = \frac{Deformed\ Length}{Undeformed\ Length}$$

$$\lambda = 1 - \varepsilon \quad (8)$$

ε - Representing the strain in the material.

The three invariants specifically represent the change in length, surface area and volume of the hyper-elastic material.

Since the material is assumed to be incompressible, therefore:

$$\lambda_1\lambda_2\lambda_3 = 1 \quad (9)$$

Mooney-Rivlin model: The Mooney-Rivlin model uses a linear combination of two invariants of the Cauchy-Green deformation tensor in the definition of the strain energy density function (W) which is defined as follows:

$$W = C_1(I_1 - 3) + C_2(I_2 - 3) \quad (10)$$

For the case of uniaxial tension or compression imparted to the O-ring, the following values can be used:

$$\lambda_1 = \lambda \quad (11)$$
$$\lambda_2 = \frac{1}{\sqrt{\lambda}} \quad (12)$$
$$\lambda_3 = \frac{1}{\sqrt{\lambda}} \quad (13)$$

Using these values

$$I_1 = \lambda^2 + \frac{2}{\lambda} \quad (14)$$
$$I_2 = \lambda + \frac{2}{\lambda^2} + \lambda \quad (15)$$

On substituting these values in Eq. (10),

$$W = C_1\left(\lambda^2 + \frac{2}{\lambda} - 3\right) + C_2\left(\lambda + \frac{1}{\lambda^2} + \lambda - 3\right) \quad (16)$$

The differentiation of the above equation with respect to λ yields the value of stress. Therefore, on differentiating with respect to λ, we have:

$$\frac{dW}{d\lambda} = C_1\left(2\lambda - \frac{2}{\lambda^2}\right) + C_2\left(2 - \frac{2}{\lambda^3}\right) \quad (17)$$
$$f = \frac{dW}{d\lambda} = 2\,C_1\left(\lambda - \frac{1}{\lambda^2}\right) + 2C_2\left(1 - \frac{1}{\lambda^3}\right) \quad (18)$$
$$f = 2\,(C_2 + C_1\lambda)\left(1 - \frac{1}{\lambda^3}\right) \quad (19)$$

Equation (2.11) can be rewritten as

$$f = 2\,\left(C_1 + \frac{C_2}{\lambda}\right)\left(\lambda - \frac{1}{\lambda^2}\right) \quad (20)$$

Where 'f' denotes the Cauchy stress and C_2 *and* C_1 are material constants. The values of material constant are estimated by curve fitting the stress (f) and stretch (λ) values from the obtained experimental results. In the present work least-square method is adopted for curve fitting the stress and stretch values. The detail discussion of the method opted is discussed in detail below. The least squared approach is based upon the minimization of the square of the error between the function and estimated values.

For example, in the present case

$$2\left(C_1+\frac{C_2}{\lambda}\right)\left(\lambda-\frac{1}{\lambda^2}\right)$$

is the function and stress "*f*" is the estimated value. Therefore, the equation (20) can be rewritten as:

$$minimize\ err = \sum_{i=1}^{n}\left(f_i-2\left(C_1+\frac{C_2}{\lambda}\right)\left(\lambda-\frac{1}{\lambda^2}\right)\right)^2 \quad (21)$$

$$minimize\ err = \sum_{i=1}^{n}\left(f_i-2\left(C_1\lambda+C_2-\frac{C_1}{\lambda^2}-\frac{C_2}{\lambda^3}\right)\right)^2 \quad (22)$$

Where

err –the error involved while curve fitting

i – Current data point being summed

n – No. of data points given

f_i – Stress at data point *i* [MPa]

Now calculate the derivatives of the function "*err*" (i.e. equation (22)) with respect to the two constants C_1 and C_2, and set both these equations equal to zero.

$$\frac{\partial err}{\partial C_1}=\left(\sum_{i=1}^{n}-2\left(f_i-2\left(C_1\lambda_i+C_2-\frac{C_1}{\lambda_i^2}-\frac{C_2}{\lambda_i^3}\right)\right)2\left(\lambda_i-\frac{1}{\lambda_i^2}\right)\right)=0 \quad (23)$$

$$\frac{\partial err}{\partial C_2}=\left(\sum_{i=1}^{n}-2\left(f_i-2\left(C_1\lambda_i+C_2-\frac{C_1}{\lambda_i^2}-\frac{C_2}{\lambda_i^3}\right)\right)2\left(1-\frac{1}{\lambda_i^3}\right)\right)=0 \quad (24)$$

Rewriting the above two equations, we obtain:

$$\sum^{n}{}_{i=1} f_i\left(\lambda_i-\frac{1}{\lambda_i^2}\right)-2C_1\sum_{i=1}^{n}\left(\lambda_i^2-\frac{2}{\lambda_i}+\frac{1}{\lambda_i^4}\right)-2C_2\sum_{i=1}^{n}\left(\lambda_i-\frac{2}{\lambda_i^2}+\frac{1}{\lambda_i^5}\right)0 \quad (25)$$

$$\sum_{i=1}^{n} f_i\left(1-\frac{1}{\lambda_i^3}\right)-2C_1\sum_{i=1}^{n}\left(\lambda_i-\frac{2}{\lambda_i^2}+\frac{1}{\lambda_i^5}\right)-2C_2\sum_{i=1}^{n}\left(n-\frac{2}{\lambda_i^3}+\frac{1}{\lambda_i^6}\right)=0 \quad (26)$$

Simultaneously solving equations 25 and 26 by substituting the values of '*f*' and 'λ', the values of C_1 and C_2 are obtained. The values of stress obtained using the Mooney-Rivlin model has been calculated above.

Apart from the Mooney-Rivlin model, there are two other models available to estimate the Young's Modulus using the Stress vs Stretch plot (i) Hooke's model and (ii) Neo-Hookean Model.

Hooke's model: Hooke's law states that the stress is proportion to the stretch and the relation between the two has been shown in equation (27).

$$f = C_{10}\,\lambda \quad (27)$$

Where,

f= Stress value and

λ= Stretch value.

The values of stress obtained using the Hooke's model has been calculated.

Neo-Hookean model: Neo-Hookean model is a hyper elastic material model that can be used for predicting the stress-strain behavior of materials, and the model is similar to Hooke's law. The strain energy density function is described as follows:

$$W = C_{10}(I_1-3) \quad (28)$$

The O-ring is assumed to be incompressible, therefore, using the Cauchy Stress Invariant I_3, is given by:

$$\lambda_1\lambda_2\lambda_3 = 1 \quad (29)$$

For the case of uniaxial tension or compression imparted to the O-ring the following values are used:

$$\lambda_1 = \lambda \quad (30)$$

$$\lambda_2 = \frac{1}{\sqrt{\lambda}} \quad (31)$$

$$\lambda_3 = \frac{1}{\sqrt{\lambda}} \quad (32)$$

Therefore, the Strain Energy Density function can be written as:

$$W = C_{10}(\lambda^2+\frac{2}{\lambda}-3) \quad (33)$$

For an incompressible Neo-Hookean material, therefore, differentiating the strain energy density function with respect to λ.

$$f = 2C_{10}\left(\lambda-\frac{1}{\lambda^2}\right) \quad (34)$$

C_{10}= Material constant (Neo-Hookean constant)

The value of Neo-Hookean constant can be determined from the above equation. The values of Neo-Hookean constant should be determined for each case and average value must be taken as Neo-Hookean constant. The values of stress obtained using the Neo-Hookean model is thus determined.

3. Experimental Validation

Two sets of stress vs strain experimental data for materials "AN 70 O-ring at 165˚C" and "GLS 70 at 175˚C" were obtained under both compression and tension conditions. The specimen height was 50mm and cross-sectional area of 635mm². The details of the experimental results and different models are discussed below. When the O-ring is placed inside the assembly, a part of the O-ring will undergo compression as a result of the applied load whereas the other part of the O-ring will suffer from tensile stress; therefore, both these modes have been considered in the analysis of the above proposed models.

Compression Mode: The values obtained for AN 70 O-ring are tabulated in Table 1. Deformation of specimen is from 2%-32% of its total length. To obtain elastic constant from Hooke's law, average value of force in each case was calculated.

The stretch ratio λ is a fundamental quantity to describe material deformation. It is defined as the current length (deformed length) divided by the original length (50mm). Stress values are calculated from the equation,

$$\text{Stress} = \frac{average\ value\ of\ force}{initial\ cross\ sectional\ area} \quad (35)$$

Strain values are calculated from the equation,

$$\text{Strain} = \frac{final\ length - initial\ length}{initial\ length} \quad (36)$$

From these stress-strain values elastic constants are determined from *Hooke's law*,

$$E = \frac{stress}{strain} \quad (37)$$

From the values of elastic constants, the specimen elastic constant is determined by taking the average value of elastic constants from each case. Value of elastic constant in this case is: 24.3031.

The constants for the Neo-Hookean and Mooney-Rivlin models were predicted using curve fit method using Eq. (21) and (22) respectively. The estimated value of constants and the stress values are shown in table 2.

Table 1: Experimental Stress-strain values

Trial 1 (N)	Trial 2 (N)	Average force(N)	% of total height	Deformation(mm)	Deformed length	Stretch	Stress (MPa)	Strain	Elastic constant (MPa)
291.3	284.4	287.85	2%	1	49	0.98	0.453	0.02	22.6654
734.5	723.7	729.1	5%	2.5	47.5	0.95	1.148	0.05	22.6654
1499.4	1483.7	1491.55	10%	5	45	0.9	2.348	0.1	23.489
2294.8	2274.2	2284.5	15%	7.5	42.5	0.85	3.597	0.15	23.9843
3143.0	3108.7	3125.85	20%	10	40	0.8	4.922	0.2	24.613
4050.0	4012.9	4031.45	25%	12.5	37.5	0.75	6.348	0.25	25.395
5511.3	5466.2	5488.75	32%	16	34	0.68	8.643	0.32	27.0116

Table 2: Estimated value of constants and the stress values

Neo-Hookean constant	Mooney-Rivlin constants	Intermediate values of deformation (mm)	Deformed length (mm)	Stretch	Strain	Neo-Hookean stress (MPa)	Mooney Rivlin stress (MPa)	Hooks law (MPa)
-3.7015	C_{10}=-5.12	3	47	0.94	0.06	1.2843	1.3501	1.46
-3.632	C_{01}=1.509	4	46	0.92	0.08	1.7514	1.8229	1.94
-3.5103		6	44	0.88	0.12	2.7551	2.8062	2.91
-3.3681		8	42	0.84	0.16	3.8664	3.8439	3.89
-3.2279		9	41	0.82	0.18	4.469	4.3846	4.37
-3.0886		11	39	0.78	0.22	5.7849	5.5125	5.34
-2.915		13	37	0.74	0.26	7.2752	6.7055	6.31
		14	36	0.72	0.28	8.0981	7.327	6.80
		15	35	0.7	0.3	8.9809	7.9652	7.29

Comparison of stretch values for different values of stresses of experimental and intermediate values for all three models are plotted in figure 3. From this figure it can be observed that Mooney-Rivlin model estimates the value closest to the experimental value.

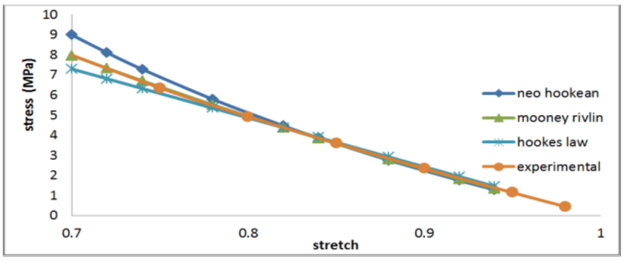

Fig. 3 Comparison of stress vs stretch for AN 70 under compression

The test was repeated for GLS 70 O-Ring at 175°C in compression mode. The comparison of the results is shown in figure 4.

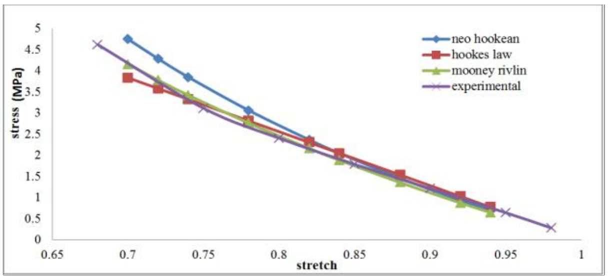

Fig. 4 Comparison of stress vs stretch for GLS 70 under compression

Tension Mode: The similar test was repeated for samples in tension. The comparison of result is shown in figure 5(a) and (b) for AN 70 and GLS 70 respectively.

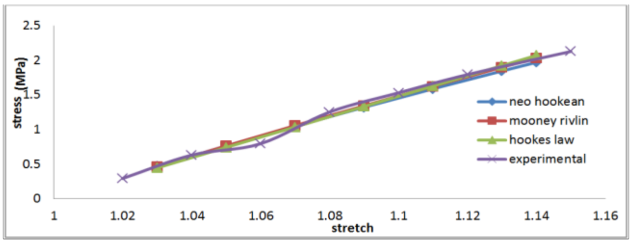

(a) AN 60

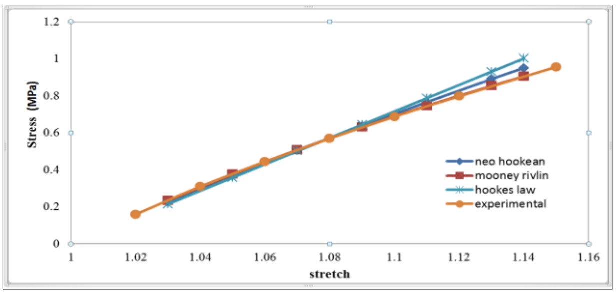

(b) GLS 70

Fig. 5 Comparison of stress vs stretch for in-tension mode

It is inferred from the above plots that Mooney-Rivlin model is the best model which describes the behavior of materials in tension and compression compared to other theoretical models. Hence in the present work, Mooney-Rivlin model is used to estimate Young's Modulus.

Contact Width: Compression applied to the O-ring causes it to deform along the groove surface. The contact width thereafter generated has been described as a function of the squeeze imposed on the O-ring. The absence of the restraining effects of the lateral walls allows for the expansion of the O-ring along the radial direction.

$$Contact\ Width = 1.5 * \psi^{2/3} \quad (38)$$

Load per unit length: The elastic reaction of the O-ring under deformation, is the prime reason for the utilization of the O-ring for sealing purposes. With the increase in the compression within elastic limits, the load per unit length can be easily estimated as a function of the Young's Modulus cross-section diameter and the squeeze of the O-ring.

$$L = E * d * (1.25 * \psi^{1.5} + 50 * \psi^{6}) \quad (39)$$

After calculating the load per unit length, the total compressive force can be estimated by multiplying the load per unit length with the circumferential length ($\pi * D$). This is represented in eq. (40).

$$Comp\_Force = \pi * L * D \quad (40)$$

Average stress over the O-ring: The primary sealing feature of an O-ring is the generation of contact stress upon deformation, which will be distributed over the contact width generated as a result of compression. The average stress can be evaluated using:

$$Stress = E * \sqrt{\frac{8}{3\pi} * \left[1.25 * \psi^{1.5} + 50 * \psi^{6}\right]} \quad (41)$$

Peak contact stress: The contact stress generated will be distributed in such a way that the maximum stress generated will be at the center of the contact width which will be evaluated using eq. (42).

$$MaxContStress = \left(E(2.62\psi - 8.85\,\psi^2 + 12.83\,\psi^3)\right) \quad (42)$$

The internal fluid sealed by the O-ring will exert pressure on the O-ring, thereby, deforming it further. This consequent deformation will result in increased contact pressure generation by the O-ring. This stress is known as hydro-stress and is expressed as the product of Poisson's ratio times the fluid pressure. This increase is calculated using eq. (43).

$$Hydrostress = \upsilon * P_1 \quad (43)$$

$$MaxContStressfluid = (E(2.62\psi - 8.85\,\psi^2 + 12.83\,\psi^3) + \upsilon * P_1) \quad (44)$$

4. Axially Loaded Lubricated Condition

Lubrication is provided to the O-ring in order to increase the life of the O-ring safeguarding the O-ring against wear and fatigue. When lubrication is provided to an O-ring, the fluid will tend to swell up the O-ring which will result in the increase in cross-section diameter of the O-ring. The increased diameter is then calculated taking into consideration the percentage of swell (sw) and thereafter using eq. (44).

$$d_1 = d\sqrt{1 + 0.01Sw} \quad (44)$$

Squeeze for lubricated O-ring after loading: With the change in diameter, the equivalent squeeze also changes and therefore, it is calculated using eq. (45).

$$squeeze = \psi * d_1 \quad (45)$$

Load per unit length for lubricated O-ring: The load changes with the change in the cross-sectional diameter and is given by the expression below:

$$L = E * d_1 * (1.25 * \psi^{1.5} + 50 * \psi^6) \quad (46)$$

After calculating the load per unit length, the total compressive force can be estimated by multiplying the load per unit length with the circumference ($\pi * D$). This is represented in eq. (47).

$$Comp\_Force = \pi * L * D \quad (47)$$

The contact width and the contact stress generated for the O-ring have the same formula's which have been covered in Eq. (38), (41), (42), (43) and (44) respectively.

5. Radially Loaded O-Ring

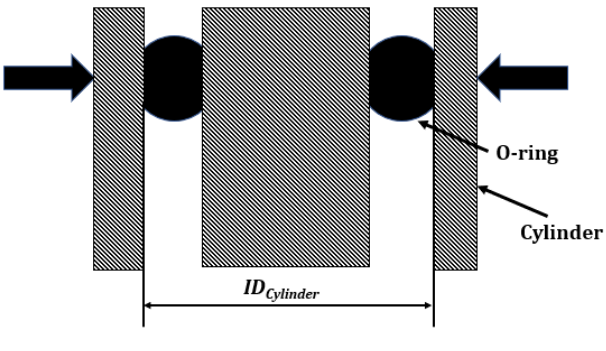

Fig. 6 Radial O-ring without Groove

The arrangement for the radial no groove arrangement is depicted in figure (6). The arrangement functions such that the O-ring is free to expand axially as a result of which the corresponding shape of the O-ring under load changes to the figure 7, given below:

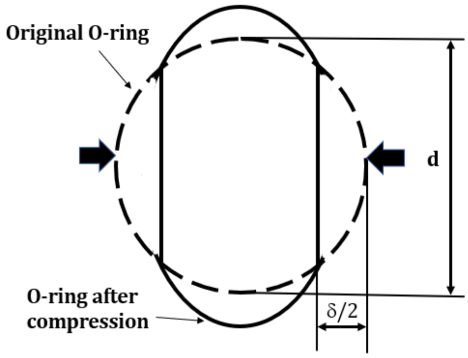

Fig. 7 Deformed shape of O-ring

The applied compression on the O-ring will result in the change in the cross-section of the O-ring as shown in figure (7). In order to define the change in the O-ring shape, a parameter called as Compression ratio (ψ) is introduced which is defined as the change in the cross-sectional diameter divided by the original cross-sectional diameter.

$$\psi = \frac{Change\ in\ cross-sectional\ diameter}{Original\ diameter} \quad (48)$$

There are two possible installations of the O-ring into the assembly: (i) Unlubricated condition and (ii) Lubricated condition. Both of these conditions have been discussed separately.

6. Radially Loaded Unlubricated Condition

The unlubricated condition pertains to the installation of the O-ring inside the assembly without lubrication being provided to its surface. For static applications, where the movement between the sealing faces and the O-ring surface is negligible, unlubricated O-rings do not drastically affect the life of the O-ring.

Inner Diameter of the O-ring: The initial requirement are the inner diameter of the cylinder and the distance between the sealing faces for the calculation of the inner diameter of the O-ring.

$$ID_{O-ring} = ID_{Cylinder} - 2C \quad (49)$$

Squeeze: The O-ring under compression will undergo an effective squeeze which is calculated from the product of compression ratio (ψ) and O-ring diameter (d). The formulation is given in equation (50).

$$squeeze = \psi * d \quad (50)$$

Young's Modulus (E): The Young's Modulus for the O-ring can be calculated using two methods: (i) Using hardness and (ii) Using Stress-Strain values. Both of these methods have been discussed in detail earlier
Contact Width: The contact width is a function of the squeeze imposed on the O-ring. Contact width generated increases with the increase in the compression ratio and is given by eq. (51).

$$Contact\ Width = 1.5 * \psi^{2/3} \quad (51)$$

Load per unit length: With the increase in the compression within elastic limits, the load per unit length can be easily estimated as a function of the Young's Modulus cross-section diameter and the compression ration of the O-ring.

$$L = E * d * (1.25 * \psi^{1.5} + 50 * \psi^{6}) \quad (52)$$

After calculating the load per unit length, the total compressive force can be estimated by multiplying the load per unit length with the circumference ($\pi * D$). This is represented in eq. (53).

$$Comp\_Force = \pi * L * D \quad (53)$$

Average stress over the O-ring: The contact stress generated will be distributed over the contact width. The average stress can be evaluated using:

$$Stress = E * \sqrt{\frac{8}{3\pi} * [1.25 * \psi^{1.5} + 50 * \psi^{6}]} \quad (54)$$

Peak contact stress: The contact stress generated will be distributed in such a way that the maximum stress generated will be at the center of the contact width which will be evaluated using eq. (55).

$$MaxContStress = \left(E(3.4\psi - 11.28\,\psi^2 + 21.75\,\psi^3)\right) \quad (55)$$

The sealed fluid pressure further deforms the O-ring and due to the elastic nature of the material, it results in an increase in the contact stress thereafter generated. This increase is calculated using eq. (56).

$$Hydrostress = \upsilon * P_1 \quad (56)$$

$$MaxContStressfluid = (E(3.4\psi - 11.28\,\psi^2 + 21.75\,\psi^3) + \upsilon * P_1) \quad (57)$$

7. Radially Loaded Lubricated Condition

When lubrication is provided to an O-ring, the fluid will tend to swell up the O-ring which will results in the increase in cross-section diameter of the O-ring. The increased diameter is then calculated taking into consideration the percentage of swell (sw) and thereafter using eq. (58).

$$d_1 = d\sqrt{1 + 0.01Sw} \quad (58)$$

Squeeze under lubricated conditions: With the change in diameter, the equivalent squeeze also changes and therefore, is calculated using eq. (59).

$$squeeze = \psi * d_1 \quad (59)$$

Load per unit length under lubrication: With the provision for the lubrication of the O-ring, the load per unit length acting on the O-ring will vary as it is a function of the cross-section diameter of the O-ring. With the increase in the compression within elastic limits, the load per unit length can be easily estimated as a function of the Young's Modulus cross-section diameter and the squeeze of the O-ring.

$$L = E * d_1 * (1.25 * \psi^{1.5} + 50 * \psi^{6}) \quad (60)$$

After calculating the load per unit length, the total compressive force can be estimated by multiplying the load per unit length with the circumference ($\pi * D$). This is represented in eq. (61).

$$Comp\_Force = \pi * L * D \quad (61)$$

The contact width and the contact stress generated for the O-ring have the same formula's which have been covered in Eq. (51), (54), (55), (56) and (57) respectively.

Conclusion

In this paper, the design of the O-ring inside a no groove assembly has been considered. Both axial as well as radial loading of the O-ring has been taken into consideration with the case of a lubricated O-ring dealt with separately for each case. The design includes the calculation of the compression imposed upon the O-ring following which the values of the contact width, contact stress, and Young's Modulus were estimated. The effect of the sealed fluid pressure on the contact stress was also taken into consideration. Various tolerances involved during the design process were also incorporated.

References

[1]. P. Hannifin, *The Parker O-ring Handbook*. Pradifa.

[2]. Flitney, *Seals and Sealing Handbook*, Sixth. Butterworth-Heinemann, 2014.

[3]. Green and C. English, "Stresses and Deformation of Compressed Elastomeric O-Ring Seals," *14th Int. Conf. Fluid Seal.*, no. April, pp. 83–95, 1994.

[4]. H. Hirani, "Online Wear monitoring of Spur Gears," *Indian J. Tribol.*, vol. 4(2), pp. 38–43, 2009.

[5]. K. P. Lijesh, D. Kumar, S. M. Muzakkir, and H. Hirani, "Thermal and frictional performance evaluation of nano lubricant with multi wall carbon nano tubes (MWCNTs) as nano-additive," *AIP Conf. Proc.*, vol. 1953, no. May, pp. 1–6, 2018.

[6]. H. Hirani, "Online Condition Monitoring of High Speed Gears Using Vibration and Oil Anlyses," in *Thermal, Fluid and Manufacturing Sciences*, New Delhi: Narosa publishing House, 2012

[7]. H. Hirani and P. Samanta, "Test setup for magneto hydrodynamic journal bearing," in *NaCoMM-2005*, 2005, pp. 298–303.

[8]. C. Sarkar and H. Hirani, "Synthesis and characterisation of nano silver particle-based magnetorheological fluids for brakes," *Def. Sci. J.*, vol. 65, no. 3, pp. 252–258, 2015.

[9]. H. Hirani and C. S. Manjunatha, "Performance evaluation of a magnetorheological fluid variable valve," *Proc. Inst.*

Mech. Eng. Part D J. Automob. Eng., vol. 221, no. 1, pp. 83–93, 2007.

[10]. F. Authors, "Experimental studies on Magnetorheological Brake containing Plane, Holed and Slotted Discs Article information : Users who downloaded this article also downloaded : About Emerald www.emeraldinsight.com," *Ind. Lubr. Tribol.*, vol. 69, no. 2, 2016.

[11]. K. P. Lijesh and H. Hirani, "Design of Eight Pole Radial Active Magnetic Bearing using Monotonicity," in *IcIIS Conference*, 2015, no. April.

[12]. H. Hirani, K. Athre, and S. Biswas, "A Hybrid Solution Scheme for Performance Evaluation of Crankshaft Bearings," *J. Tribol.*, vol. 122, no. October, pp. 733–740, 2000.

[13]. P. Samanta and H. Hirani, "A simplified Optimization Approach for Permanent Magnetic Journal Bearing," *Indian J. Tribol.*, vol. 2, no. 2, pp. 23–28, 2007.

[14]. H. Hirani and S. S. Goilkar, "Tribological Characterization of Carbon Graphite Secondary Seal," *Indian J. Tribol.*, vol. 4(2), pp. 1–6, 2009.

[15]. K. P. Lijesh and H. Hirani, "Failure mode and effect analysis of active magnetic bearings," *Tribol. Ind.*, vol. 38, no. 1, pp. 90–101, 2016.

[16]. H. Hirani and S. S. Goilkar, "Rotordynamic Analysis of Carbon Graphite Seals of a Steam Rotary Joint," in *IuTAM Symposium on Emerging Trends in Rotor Dynamics*, 2011, pp. 253–262.

[17]. S. P. S. Padala, J. U. Maheswari, and H. Hirani, "Identification and classification of change causes and effects in construction projects," *Int. J. Constr. Manag.*, vol. 0, no. 0, pp. 1–20, 2020.

[18]. M. Prudhvi Krishna *et al.*, "Effectiveness of different facemask materials to combat transmission of airborne diseases," *Sadhana - Acad. Proc. Eng. Sci.*, vol. 46, no. 3, Sep. 2021.

[19]. P. Kumar and H. Hirani, "Misalignment effect on gearbox failure: An experimental study," *Meas. J. Int. Meas. Confed.*, vol. 169, no. September 2020, p. 108492, 2021.

[20]. H. Hirani, T. V. V. L. N. Rao, K. Athre, and S. Biswas, "Rapid performance evaluation of journal bearings," *Tribol. Int.*, vol. 30, no. 11, pp. 825–834, 1997.

[21]. H. Hirani, "Theoretical and experimental studies on design of dynamically loaded journal bearing," 1998.

[22]. H. Hirani, K. Athre, and S. Biswas, "Rapid and globally convergent method for dynamically loaded journal bearing design," *Proc. Inst. Mech. Eng. Part J J. Eng. Tribol.*, vol. 212, no. 3, pp. 207–213, 1998.

[23]. H. Hirani, K. Athre, and S. Biswas, "Length Journal Bearings : Analytical Method of Solution - (I)," *J. Tribol.*, vol. 121, no. October, 1999.

[24]. H. Hirani, K. Athre, and S. Biswas, "Dynamic analysis of engine bearings," *Int. J. Rotating Mach.*, vol. 5, no. 4, pp. 283–293, 1999.

[25]. T. V. V. L. N. Rao, S. Biswas, H. Hirani, and K. Athre, "An analytical approach to evaluate dynamic coefficients and nonlinear transient analysis of a hydrodynamic journal bearing," *Tribol. Trans.*, vol. 43, no. 1, pp. 109–115, 2000.

[26]. H. Hirani, K. Athre, and S. Biswas, "Comprehensive design methodology for an engine journal bearing," *Proc. Inst. Mech. Eng. Part J J. Eng. Tribol.*, vol. 214, no. 4, pp. 401–412, 2000.

[27]. H. Hirani, K. Athre, and S. Biswas, "A Simplified Mass Conserving Algorithm for Journal Bearing under Large Dynamic Loads," *Int. J. Rotating Mach.*, vol. 7, no. 1, pp. 41–51, 2001.

[28]. H. Hirani, K. Athre, and S. Biswas, "Lubricant shear thinning analysis of engine journal bearings," *Tribol. Trans.*, vol. 44, no. 1, pp. 125–131, 2001.

[29]. H. Hirani and T. V. V. L. N. Rao, "Optimization of Journal Bearing Groove Geometry Using Genetic Algorithm," *NaCoMM03, IIT Delhi, India*, vol. 1, pp. 1–9, 2003.

[30]. R. K. Burla, P. Seshu, H. Hirani, P. R. Sajanpawar, and H. S. Suresh, "Three dimensional finite element analysis of crankshaft torsional vibrations using parametric modeling techniques," *SAE Tech. Pap.*, no. March 2020, 2003.

[31]. H. Hirani, "Multiobjective optimization of a journal bearing using the Pareto optimality concept," *Proc. Inst. Mech. Eng. Part J J. Eng. Tribol.*, vol. 218, no. 4, pp. 323–336, 2004.

[32]. H. Hirani and P. Samanta, "Performance evaluation of magnetohydrodynamic bearing," *Proc. World Tribol. Congr. III - 2005*, pp. 97–98, 2005.

[33]. H. Hirani and N. P. Suh, "Journal bearing design using multiobjective genetic algorithm and axiomatic design approaches," *Tribol. Int.*, vol. 38, no. 5, pp. 481–491, 2005.

[34]. H. Hirani, "Multiobjective optimization of journal bearing using mass conserving and genetic algorithms," *Proc. Inst. Mech. Eng. Part J J. Eng. Tribol.*, vol. 219, no. 3, pp. 235–248, 2005.

[35]. H. Hirani and P. Samanta, "Hybrid (hydrodynamic + permanent magnetic) journal bearings," *Proc. Inst. Mech. Eng. Part J J. Eng. Tribol.*, vol. 221, no. 8, pp. 881–891, 2007.

[36]. V. K. Sukhwani and H. Hirani, "Synthesis and characterization of low cost magnetorheological (MR) fluids," *Behav. Mech. Multifunct. Compos. Mater. 2007*, vol. 6526, p. 65262R, 2007.

[37]. P. Samanta and H. Hirani, "Magnetic Bearing Configurations: Theoretical and Experimental Studies," *IEEE Trans. Magn.*, vol. 44, no. 2, pp. 292–300, Feb. 2008.

[38]. V. K. Sukhwani and H. Hirani, "Design, development, and performance evaluation of high-speed magnetorheological brakes," *Proc. Inst. Mech. Eng. Part L J. Mater. Des. Appl.*, vol. 222, no. 1, pp. 73–82, 2008.

[39]. V. K. Sukhwani and H. Hirani, "A Comparative Study of Magnetorheological-Fluid-Brake and Magnetorheological-Grease-Brake," *Tribol. Online*, vol. 3, no. 1, pp. 31–35, 2008.

[40]. H. Hirani and M. Verma, "Tribological study of elastomeric bearings for marine propeller shaft system," *Tribol. Int.*, vol. 42, no. 2, pp. 378–390, 2009.

[41]. H. Hirani and S. S. Goilkar, "Formation of transfer layer and its effect on friction and wear of carbon-graphite face seal under dry, water and steam environments," *Wear*, vol. 266, no. 11–12, pp. 1141–1154, 2009.

[42]. H. Hirani, "Root cause failure analysis of outer ring fracture of four-row cylindrical roller bearing," *Tribol. Trans.*, vol. 52, no. 2, pp. 180–190, 2009.

[43]. S. S. Goilkar and H. Hirani, "Design and development of a test setup for online wear monitoring of mechanical face seals using a torque sensor," *Tribol. Trans.*, vol. 52, no. 1, pp. 47–58, 2009.

[44]. S. S. Goilkar and H. Hirani, "Parametric study on balance ratio of mechanical face seal in steam environment," *Tribol. Int.*, vol. 43, no. 5–6, pp. 1180–1185, 2010.

[45]. S. Gupta and H. Hirani, "Optimization of magnetorheological brake," *Am. Soc. Mech. Eng. Tribol. Div. TRIB*, pp. 405–406, 2011.

[46]. S. Verma, V. Kumar, and K. D. Gupta, “Performance analysis of flexible multirecess hydrostatic journal bearing operating with micropolar lubricant,” *Lubr. Sci.*, vol. 24, no. 6, pp. 273–292, 2012.
[47]. C. Sarkar and H. Hirani, “Theoretical and experimental studies on a magnetorheological brake operating under compression plus shear mode,” *Smart Mater. Struct.*, vol. 22, no. 11, 2013.
[48]. C. Sarkar and H. Hirani, “Design of a squeeze film magnetorheological brake considering compression enhanced shear yield stress of magnetorheological fluid,” *J. Phys. Conf. Ser.*, vol. 412, no. 1, 2013.
[49]. C. Sarkar and H. Hirani, “Synthesis and characterization of antifriction magnetorheological fluids for brake,” *Def. Sci. J.*, vol. 63, no. 4, pp. 408–412, 2013.
[50]. H. Shah and H. Hirani, “Online condition monitoring of spur gears,” *Int. J. Cond. Monit.*, vol. 4, no. 1, pp. 15–22, 2014.
[51]. K. P. Lijesh and H. Hirani, “Design and development of Halbach electromagnet for active magnetic bearing,” *Prog. Electromagn. Res. C*, vol. 56, pp. 173–181, 2015.
[52]. K. P. Lijesh and H. Hirani, “Optimization of Eight Pole Radial Active Magnetic Bearing,” *J. Tribol.*, vol. 137, pp. 0245021–7, 2015.
[53]. P. Kumar, H. Hirani, and A. Agrawal, “Scuffing behaviour of EN31 steel under dry sliding condition using pin-on-disc machine,” *Mater. Today Proc.*, vol. 2, no. 4–5, pp. 3446–3452, 2015.
[54]. Sarkar and H. Hirani, “Synthesis and characterization of nano-particles based magnetorheological fluids for brake,” *Tribol. Online*, vol. 10, no. 4, pp. 282–294, 2015.
[55]. K. P. Lijesh and H. Hirani, “Development of analytical equations for design and optimization of axially polarized radial passive magnetic bearing,” *J. Tribol.*, vol. 137, no. 1, pp. 1–10, 2015
[56]. C. Sarkar and H. Hirani, “Effect of Particle Size on Shear Stress of Magnetorheological Fluids,” *Smart Sci.*, vol. 3, no. 2, pp. 65–73, 2015.
[57]. C. Sarkar and H. Hirani, “Development of a magnetorheological brake with a slotted disc,” *Proc. Inst. Mech. Eng. Part D J. Automob. Eng.*, vol. 229, no. 14, pp. 1907–1924, 2015.
[58]. K. P. Lijesh and H. Hirani, “Magnetic bearing using rotation magnetized direction configuration,” *J. Tribol.*, vol. 137, no. 4, 2015.
[59]. K. P. Lijesh and H. Hirani, “Modeling and development of RMD configuration magnetic bearing,” *Tribol. Ind.*, vol. 37, no. 2, pp. 225–235, 2015.
[60]. C. Desai, H. Hirani, and A. Chawla, “Life Estimation of Hip Joint Prosthesis,” *J. Inst. Eng. Ser. C*, vol. 96, no. 3, pp. 261–267, 2015.
[61]. K. P. Lijesh, S. M. Muzakkir, H. Hirani, and G. D. Thakre, “Control on wear of journal bearing operating in mixed lubrication regime using grooving arrangements,” *Ind. Lubr. Tribol.*, vol. 68, no. 4, pp. 458–465, 2016.
[62]. K. P. Lijesh and H. Hirani, “Design and Development of Permanent Magneto-Hydrodynamic Hybrid Journal Bearing,” *J. Tribol.*, vol. 139, no. 4, 2017.
[63]. P. Kumar, H. Hirani, and A. Agrawal, “Fatigue failure prediction in spur gear pair using AGMA approach,” *Mater. Today Proc.*, vol. 4, no. 2, pp. 2470–2477, 2017.
[64]. K. P. Lijesh, D. Kumar, and H. Hirani, “Effect of disc hardness on MR brake performance,” *Eng. Fail. Anal.*, vol. 74, pp. 228–238, 2017.
[65]. K. P. Lijesh, D. Kumar, and H. Hirani, “Synthesis and field dependent shear stress evaluation of stable MR fluid for brake application,” *Ind. Lubr. Tribol.*, vol. 69, no. 5, pp. 655–665, 2017.
[66]. P. Kumar, H. Hirani, and A. K. Agrawal, “Online condition monitoring of misaligned meshing gears using wear debris and oil quality sensors,” *Ind. Lubr. Tribol.*, vol. 70, no. 4, pp. 645–655, 2018.
[67]. P. Kumar, H. Hirani, and A. K. Agrawal, “Modeling and Simulation of Mild Wear of Spur Gear Considering Radial Misalignment,” *Iran. J. Sci. Technol. - Trans. Mech. Eng.*, vol. 43, pp. 107–116, 2019.
[68]. P. Kumar, H. Hirani, and A. Kumar Agrawal, “Effect of gear misalignment on contact area: Theoretical and experimental studies,” *Meas. J. Int. Meas. Confed.*, vol. 132, pp. 359–368, 2019.
[69]. P. Kumar, H. Hirani, and A. Kumar Agrawal, “Effect of gear misalignment on contact area: Theoretical and experimental studies,” *Measurement*, vol. 132, pp. 359–368, Jan. 2019.